NAR Genomics and Bioinformatics, 2024, **6**, 1–10
https://doi.org/10.1093/nargab/lqad113
Advance access publication date: 15 January 2024
Standard Article

OXFORD

BRD2 and *BRD3* genes independently evolved RNA structures to control unproductive splicing

Marina Petrova[1,†], Sergey Margasyuk[1,†], Margarita Vorobeva[2], Dmitry Skvortsov[1,2], Olga A. Dontsova[1,2] and Dmitri D. Pervouchine[1,*]

[1]Skolkovo Institute of Science and Technology, Bolshoy Bulvar, 30, str. 1, Moscow 121205, Russia
[2]Faculty of Chemistry, Moscow State University, GSP-1, 1-3 Leninskiye Gory, Moscow 119991, Russia

[*]To whom correspondence should be addressed. Tel: +7 495 280 14 81; Fax: +7 495 280 14 81; Email: d.pervouchine@skoltech.ru
[†]The first two authors should be regarded as Joint First Authors.

Abstract

The mammalian *BRD2* and *BRD3* genes encode structurally related proteins from the bromodomain and extraterminal domain protein family. The expression of *BRD2* is regulated by unproductive splicing upon inclusion of exon 3b, which is located in the region encoding a bromodomain. Bioinformatic analysis indicated that *BRD2* exon 3b inclusion is controlled by a pair of conserved complementary regions (PCCR) located in the flanking introns. Furthermore, we identified a highly conserved element encoding a cryptic poison exon 5b and a previously unknown PCCR in the intron between exons 5 and 6 of *BRD3*, however, outside of the homologous bromodomain. Minigene mutagenesis and blockage of RNA structure by antisense oligonucleotides demonstrated that RNA structure controls the rate of inclusion of poison exons. The patterns of *BRD2* and *BRD3* expression and splicing show downregulation upon inclusion of poison exons, which become skipped in response to transcription elongation slowdown, further confirming a role of PCCRs in unproductive splicing regulation. We conclude that *BRD2* and *BRD3* independently acquired poison exons and RNA structures to dynamically control unproductive splicing. This study describes a convergent evolution of regulatory unproductive splicing mechanisms in these genes, providing implications for selective modulation of their expression in therapeutic applications.

Introduction

The bromodomain and extraterminal domain (BET) protein family, a subgroup of the bromodomain protein superfamily (1–3), consists of four related chromatin readers (*BRD2*, *BRD3*, *BRD4* and *BRDT*) with broad specificity on transcriptional activation of immunity-associated genes (4,5). They contain two homologous tandem bromodomains, which recognize and bind acetylated lysine residues, an extraterminal (ET) domain, and two small conserved motifs located between the two bromodomains and between the second bromodomain and the ET domain (6). Abnormal expression or loss of function in BET proteins is associated with pathological processes, including immune and inflammatory diseases, and is being increasingly considered as a prominent therapeutic target (7).

BET family members have evolved in a series of duplications that occurred before vertebrate radiation (8). A high degree of sequence similarity, interactions with many of the same transcription factors (9–12) and overlapping epigenetic binding profiles (13) suggest that BET proteins have similar cellular activities. However, despite these shared characteristics, there appears to be no functional redundancy between them (14). The fact that BET members cannot compensate for each other is emphasized by the lethal consequences of *BRD2* (15) and *BRD4* (16) deletion. Unlike *BRD3*, *BRD2* does not have reprogramming activity (17) and its depletion does not lead to cell death (13). The depletion of *BRD2* but not *BRD3* or *BRD4* reverts the sigma-2 receptor upregulation induced by cholesterol deprivation (18). Yet, the molecular mechanisms underlying BET-specific functions remain largely unresolved.

The bromodomain proteins, and BET family members in particular, can be regulated at the post-transcriptional level through a mechanism called unproductive splicing, in which the messenger RNA (mRNA) is triggered to degradation by the nonsense-mediated decay (NMD) as a result of regulated alternative splicing (19). The inclusion of exon 3b, which is embedded in conserved intronic sequences, introduces a frameshift and thus a premature termination codon (PTC) in the *BRD2* transcript (20,21). Such exons are called poison exons because they are normally skipped but trigger mRNA degradation upon inclusion. Another example is the *BRD9* gene, which contains a poison exon that leads to mRNA degradation in SF3B1-mutant tumors (22). Multiple cross-regulatory unproductive splicing networks tend to evolve among paralogs often containing ultraconserved elements around poison exons (23).

In this work, we questioned whether other BET family members, which are *BRD2* paralogs, could be regulated through unproductive splicing and whether this regulation is evolutionarily conserved. We identified a previously unknown cryptic poison exon in *BRD3*, which, however, resides in a nonhomologous intron with respect to the poison exon in *BRD2*, and predicted bioinformatically that both poison exons are surrounded by pairs of conserved complementary regions (PCCRs) capable of forming stable RNA structures. Using blockage of RNA structure by antisense oligonucleotides

Received: September 21, 2023. **Revised:** December 13, 2023. **Editorial Decision:** December 19, 2023. **Accepted:** December 28, 2023
© The Author(s) 2024. Published by Oxford University Press on behalf of NAR Genomics and Bioinformatics.
This is an Open Access article distributed under the terms of the Creative Commons Attribution-NonCommercial License (http://creativecommons.org/licenses/by-nc/4.0/), which permits non-commercial re-use, distribution, and reproduction in any medium, provided the original work is properly cited. For commercial re-use, please contact journals.permissions@oup.com

(AONs) and minigene mutagenesis, we demonstrated that base pairings between these PCCRs indeed control poison exon inclusion. Furthermore, we characterized unproductive splicing patterns in these genes using panels of healthy human tissue transcriptomes from the Genotype-Tissue Expression (GTEx) project and tumor transcriptomes from the The Cancer Genome Atlas (TCGA). Finally, we described characteristic RNA structure-specific patterns in unproductive splicing response to the transcription elongation slowdown.

Materials and methods

RNA-seq data

RNA sequencing (RNA-seq) data of poly(A)$^+$ RNA obtained in the GTEx project were downloaded from dbGaP (dbGaP project 15872) in fastq format and aligned to the human genome assembly GRCh38 (hg38) using STAR aligner version 2.7.3a in paired-end mode (24) with GENCODE v42 annotation as a reference (25). The RNA-seq data in RNA Pol II slowdown experiment with α-amanitin and in RNA Pol II mutants with slow elongation rate were downloaded from Gene Expression Omnibus repositories GSE153303 and GSE63375, respectively (26,27). The gene read coverage was calculated from BAM files using the featureCounts tool from Subread package version 2.0.6 (28) in paired-end mode (-p --countReadPairs options). TPM (transcripts per million) values were calculated from the read coverage using RNAnorm package version 2.0.0. Split read counts and percent-spliced-in metrics were computed by IPSA pipeline (29) with default settings as before (30). Namely, the exon inclusion rate (Ψ) was computed as $\Psi = \text{inc}/(\text{inc} + 2\text{exc})$, where inc is the number of split reads supporting exon inclusion and exc is the number of split reads supporting exon exclusion. Ψ values with the denominator below 10 were discarded. CIRCexplorer2 pipeline version 2.3.8 was used to extract backsplice junctions from GTEx samples aligned with STAR aligner in chimeric mode (--chimOutType Junctions --chimSegmentMin 15).

Cryptic exons

To search for cryptic exons, BAM files from GTEx were processed with StringTie (31) in guided assembly mode with conservative parameters (--conservative option) using GENCODE v42 annotation. Two groups of nonterminal exons were selected from the StringTie output: (i) annotated exons and (ii) exons that do not intersect any annotated exon from GENCODE. The following metrics were computed for each exon in each sample: the read coverage per base pair, the total number of split reads supporting splice junctions connecting the exon with any annotated exon and the average phastCons score derived from the multiple alignment of 100 vertebrate genomes (32). The 15th percentiles of these metrics for group (i) were used as a cutoff for group (ii). This procedure yielded 249 cryptic (unannotated) exons with all three metrics exceeding the cutoffs chosen for group (i).

Phylogenetic analysis

To construct the phylogenetic tree, we selected the smallest orthologous group in the eggNOG database including the human proteins *BRD2*, *BRD3*, *BRD4* and *BRDT* (ENOG503CSGG for the taxon Bilateria) (33). All nodes corresponding to homologs from *Homo sapiens* and *Danio rerio* were selected. The *fs(1)h* protein from *Drosophila melanogaster* was used as an outgroup. The pruned tree was visualized with IToL web service (34). The amino acid sequences of the major protein-coding isoforms of the human BET proteins were obtained from the Ensembl database (35) and aligned using Muscle software v3.8.1551 (36). The alignment and the phylogenetic trees constructed for bromodomains 1 and 2 were visualized using Jalview editor (37).

Statistical procedures

The data were analyzed using Python version 3.8.2 and R statistics software version 3.6.3. Throughout the paper, r_p denotes the Pearson correlation coefficient. The significance of r_p values was not assessed due to a small number of observations (tissues and TCGA projects). Nonparametric tests were performed using normal approximation with continuity correction. In all figures, the significance levels of 0.05, 0.01 and 0.001 are denoted by *, ** and ***, respectively.

Cell culture and transfection

Human A549 lung adenocarcinoma cells were maintained in Dulbecco's modified Eagle's medium/Nutrient Mixture F-12 with phenol red (Thermo Fisher Scientific or Servicebio) supplemented with 10% (v/v) fetal bovine serum and 1% GlutaMAX (Thermo Fisher Scientific). All treatments were done in a 12-well plate format. A549 cells were plated at a density of 150 000 cells per well. Five hundred nanograms of wild-type (WT) or mutated minigene plasmids were transfected into A549 cells using Lipofectamine 3000 (Invitrogen) for 24 h. AON (13-mer) transfection was performed with Lipofectamine RNAiMAX (Invitrogen) in OptiMEM serum-reduced media (Gibco) for 48 h. Three hours before harvest, CHX was added to the cells, giving a final concentration of 300 μg/ml in the growth medium. Each experiment was made in at least three independent biological replicates.

Minigene construction and mutagenesis

A fragment of the human genome from exon 5 to exon 6 of the *BRD3* gene was amplified using Q5 High-Fidelity DNA Polymerase (New England Biolabs). The genomic DNA of the human A549 lung adenocarcinoma cell line was used as a template. All sequences were inserted downstream of the cytomegalovirus (CMV) promoter of the pRK5 vector. The minigene encoding *BRD3* exons 5 and 6 was made using the NEBuilder HiFi DNA Assembly Master Mix (New England Biolab). The minigene encoding *BRD2* exons 3 and 4 was constructed using the blunt-end cloning approach. Mutations in all minigenes were introduced by polymerase chain reaction (PCR)-based site-directed mutagenesis. Primers for cloning and mutagenesis are listed in Supplementary Tables S1 and S2, respectively. All constructs were confirmed by sequencing and restriction analysis.

RNA extraction

Total RNA was isolated by a guanidinium thiocyanate–phenol–chloroform method using ExtractRNA Reagent (Evrogene) or PureLink RNA Minikit (Invitrogen) (38). One thousand nanograms of total RNA was first subjected to RNase-free DNase I digestion (Thermo Fisher Scientific) at 37°C for 30 min to remove contaminating genomic DNA. Next, 500 ng of total RNA was used for complementary DNA (cDNA) synthesis using Maxima First Strand cDNA Synthesis

Kit for RT-qPCR (Thermo Fisher Scientific) to a final volume of 10 µl. cDNA was diluted 1:10 with nuclease-free water for quantitative PCR (qPCR) and reverse transcription PCR (RT-PCR) analysis.

RT-PCR and RT-qPCR

RT-PCR analysis was used to assess the ratio of splice isoforms as described elsewhere (30). qPCR reactions were performed in triplicates in a final volume of 12 µl in 96-well plates with 420 nM gene-specific primers and 2 µl of cDNA using 5X qPCRmix-HS SYBR reaction mix (Evrogen). Primers for RT-PCR and RT-qPCR are listed in Supplementary Table S3. A sample without reverse transcriptase enzyme was included as control to verify the absence of genomic DNA contamination. Amplification of the targets was carried out on CFX96 Real-Time System (Bio-Rad), with following parameters: 95°C for 2 min, followed by 45 cycles at 95°C for 30 s, 61°C for 30 s and 72°C for 30 s, ending at 72°C for 5 min. Gene and gene isoform expression change was calculated using an estimate of the amplification efficiency value. To account for the relation between pipetting error and lower copy number of template input in the reaction, we discarded all the replicates that do not reside within acceptable C_q range as described in (39).

Antisense oligonucleotides

All AONs were designed as locked nucleic acid (LNA)-based with a DNA substitution at every second nucleotide (40). Synthesis of LNA/DNA mixmers was carried out by Syntol JSC (Moscow, Russia). Sequences of AONs are listed in Supplementary Table S4.

Results

Phylogenetic analysis

A study by Paillisson *et al*. suggested that vertebrate BET family consists of four separate orthologous groups corresponding to *BRD2*, *BRD3*, *BRD4* and *BRDT*, respectively, with the highest degree of similarity between *BRD2* and *BRD4* (8). In repeating this analysis, we constructed a phylogenetic tree of bilaterian homologs of *BRD2* from eggNOG database (33), which confirmed the separation of four orthologous groups, however, suggesting the most recent divergence of *BRD2* and *BRD3*, not *BRD2* and *BRD4* (a restricted tree is shown in Figure 1A). Interestingly, zebrafish has evolved two copies of *BRD2*, while mouse maintained only one (Supplementary Figure S1). The hypothesis that the closest homolog of *BRD2* could be *BRD3* is also evidenced by the relationship between phylogeny and expression profiles of these genes (8), and by the fact that *BRD2* and *BRD3* both have a shorter C-terminal domain as compared to *BRD4* and *BRDT* (41). The phylogenetic trees derived from multiple sequence alignments of the two bromodomains also confirm the highest similarity of *BRD2* to *BRD3*, not to *BRD4* (Supplementary Figure S2).

Transcript structure and poison exons

The human *BRD2* gene spans 13 exons, with the start codon located in exon 2. The inclusion of the 92-nt-long exon 3b, which follows exon 3, causes a frameshift that generates a PTC in the downstream exon (Figure 1B). Our bioinformatic analysis indicated that exon 3b is located inside a PCCR (id 668329) formed by regions R1 and R2 with the hybridization free energy $\Delta G = -29.1$ kcal/mol (26). Although the level of nucleotide sequence variation is insufficient to estimate the significance of compensatory substitutions in R1 and R2, their boundaries strongly correlate with the evolutionary conservation profile forming two pronounced phastCons peaks, which disappear when the complementarity ends—a pattern that has been reported previously for many functional RNA structures (42).

This observation naturally led us to ask whether *BRD3*, the closest paralog of *BRD2*, also contains a poison exon. In examining the homologous part of *BRD3*, no poison exon was found in between exons 3 and 4; however, we identified a conserved element in the intron spanning between exons 5 and 6 (Figure 1C). This element represents an 82-nt-long unannotated exon 5b with the canonical GT/AG splice site consensus sequences, which is expressed at low levels in GTEx tissues, namely in muscle and colon (see the 'Materials and methods' section). Inclusion of this exon also results in a frameshift that generates a PTC downstream. Furthermore, this cryptic exon is surrounded by a pair of stand-alone phastCons peaks (regions R3 and R4) strongly resembling those observed in *BRD2*. Upon inspection of the nucleotide sequences of R3 and R4, we found that they are complementary with $\Delta G = -34.3$ kcal/mol and have a characteristic, abrupt decrease of phylo-HMM score beyond the base-paired region. Interestingly, this PCCR was not in scope of earlier studies because it fell outside the conserved RNA element track (26,43).

The multiple alignment of protein amino acid sequences of the major protein-coding human BET protein isoforms reveals a remarkable conservation of exon boundaries (Supplementary Figure S3). However, exon 3b of *BRD2* and exon 5b of *BRD3* reside in nonorthologous introns, one separating exons encoding a bromodomain and the other located in between bromodomains (Figure 2). We examined the *BRD4* transcript and found an annotated poison exon 3b, however, pertaining to yet another intron with respect to those containing poison exons in *BRD2* and *BRD3*. This poison exon lacks any conserved RNA structure in the flanking introns (Supplementary Figure S4). The last and the most distant member of the BET family, *BRDT*, neither has annotated NMD isoforms, nor contains any expressed conserved intronic element that could possibly represent a poison exon. Interestingly, the exon 3b of *BRD2* can be traced back to amphibians, while poison exons in *BRD3* and *BRD4* first appear in mammals (Supplementary Figure S5).

In sum, we identified two stable PCCRs surrounding poison exons in *BRD2* and *BRD3*, of which the latter exon has not been annotated before. These poison exons reside in introns spanning between nonhomologous protein-coding exons, which suggests their independent acquisition in the course of evolution.

RNA structure and poison exon inclusion

To test the effect of RNA structure on the inclusion of poison exons in *BRD2* and *BRD3*, we followed the strategy outlined previously (30,44). Namely, we measured splicing changes in the endogenous pre-mRNA in response to the blockage of PCCRs by AONs, and construct minigenes carrying mutated gene fragments to assess splicing outcomes in single and double mutants.

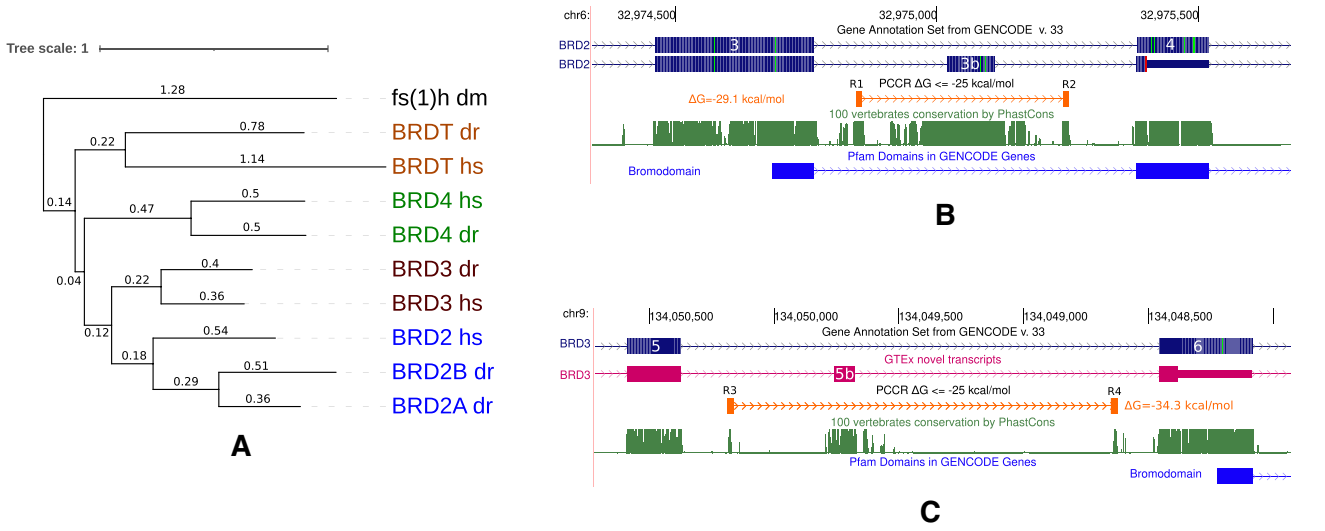

Figure 1. The BET family. (**A**) The phylogenetic tree of bilaterian homologs of *BRD2* from eggNOG database restricted to *H. sapiens* and *D. rerio*. The *fs(1)h* protein from *D. melanogaster* was used as an outgroup. The numbers on the branches denote the average number of amino acid substitutions per site. (**B**) The inclusion of exon 3b in *BRD2* results in a PTC in the downstream exon. The exon is surrounded by a PCCR formed by R1 and R2 with $\Delta G = -29.1$ kcal/mol. Exon 3b is located within a region encoding bromodomain 1. (**C**) Cryptic exon 5b in *BRD3* is unannotated and can be detected in a few human tissues, including muscle and colon. If included, it also induces a PTC downstream. It is surrounded by a PCCR formed by R3 and R4 with $\Delta G = -34.3$ kcal/mol. Exon 5b is located in between bromodomains 1 and 2.

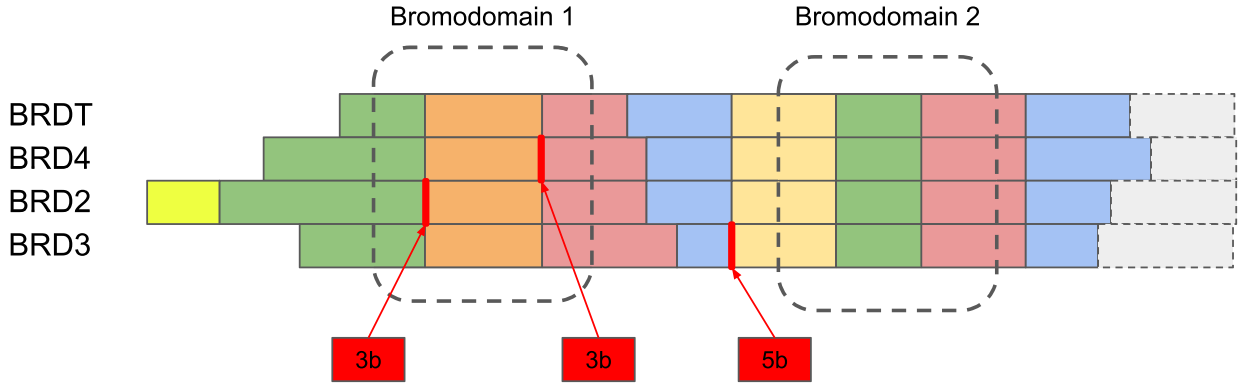

Figure 2. Conservation of exon–intron structure in the BET family. The schema represents a multiple sequence alignment of the human BET family members (full alignment in Supplementary Figure S3). Colored blocks represent different exons. Gray rectangles at the right denote the rest of the protein. Regions encoding bromodomains 1 and 2 are shown by dashed lines. Thick red vertical lines represent splice junctions corresponding to poison exons (the latter are shown as rectangles below).

First, we designed an AON complementary to the R1 sequence in *BRD2* (Figure 3A) and measured the rate of exon inclusion upon dose-dependent AON treatment by RT-PCR and qPCR. Exon 3b inclusion rate noticeably increased even at the low 25 nM concentration of AON1 (Figure 3B). To further assess the impact of RNA structure on exon 3b splicing, we repeated the AON1 treatment in the presence of NMD inhibitor cycloheximide (CHX) and measured the exon inclusion rate by qPCR. Both RT-PCR (Supplementary Figure S6A) and qPCR (Supplementary Figure S6B) confirmed a significant elevation of exon 3b inclusion upon AON1 treatment in the presence of CHX. Remarkably, the baseline inclusion rate was about 20% even when NMD was active, presumably due to the presence of nuclear fraction in the total RNA sample. We additionally analyzed the response of HeLa cell line transcriptome to UPF1/XRN1 co-depletion (45,46) and found that *BRD2* exon 3b inclusion rate increases from 16% to 40% when NMD is inactivated, which further demonstrates the poison nature of exon 3b and explains a relatively high baseline level of its inclusion.

Next, we assembled minigene constructs carrying a fragment of *BRD2* between exons 3 and 4 (Figure 3C) with single disruptive mutations and a double compensatory mutation (Figure 3D). Transfection of these constructs into A549 cells and subsequent qPCR analysis revealed that disruptive mutations (m1 and m2) significantly increased exon 3b inclusion, while the double compensatory mutation (m1m2) reversed splicing back to that of the WT (Figure 3E and F).

In *BRD3*, the treatment with AON complementary to the R3 sequence (Figure 4A) induced higher exon 5b inclusion rate, as evidenced by RT-PCR and qPCR, in the absence of CHX (Figure 4B), and a much stronger increase in the presence of CHX (Supplementary Figure S7A and B). Transfection of A549 cells with minigene constructs carrying the respective

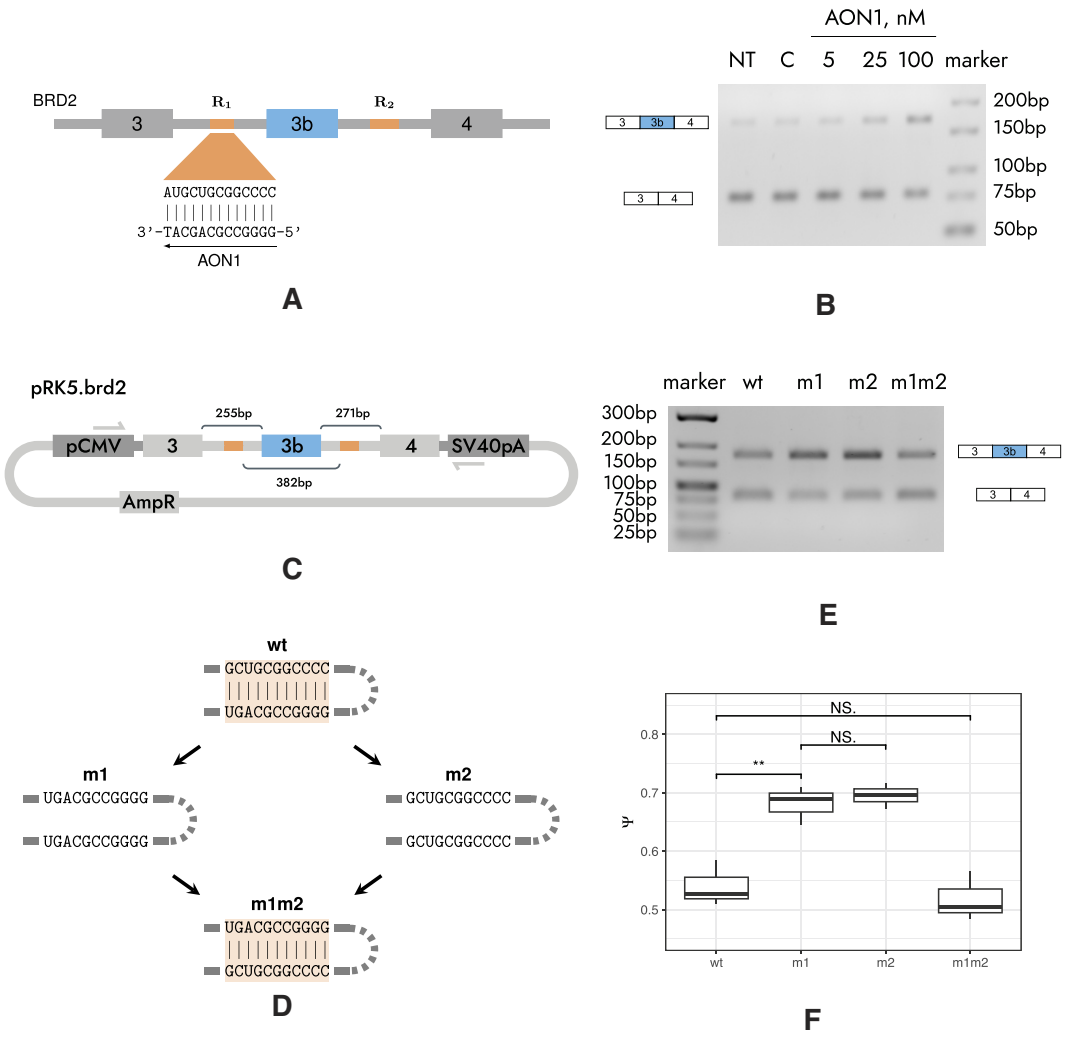

Figure 3. Validation of the RNA structure in the *BRD2* gene. (**A**) AON1 is complementary to region R1. (**B**) Exon 3b inclusion rate increases when R1/R2 base pairings are blocked by AON1. 'NT' denotes nontreated control and 'con' denotes the treatment with control AON against luciferase. AON concentrations are in nM. (**C**) The minigene pRK5.BRD2 carrying a fragment of *BRD2* between exons 3 and 4. pCMV promoter and SV40 early polyadenylation signal are shown. (**D**) Mutagenesis strategy is to create single disruptive mutants (m1 and m2) and a double compensatory mutant (m1m2). (**E**, **F**) Exon 3b inclusion rate increases in disruptive mutants but reverts to the WT in the compensatory double mutant. Asterisks (**) and NS denote statistically significant differences at the 1% significance level and not significant differences, respectively.

fragment of *BRD3* (Figure 4C) with disruptive (m3 and m4) and compensatory (m3m4) mutations (Figure 4D) again indicated that exon 5b inclusion rate increases when base pairings are disrupted, but this increase is reversed in the compensatory double mutant (Figure 4E and F). The cryptic origin of exon 5b in *BRD3* is reflected in the observation that transcript isoforms containing this exon have low expression levels. Taken together, these experiments demonstrate that base pairings within R1/R2 and R3/R4 control the rate of inclusion of *BRD2* exon 3b and *BRD3* exon 5b, respectively.

Intronic RNA structures are often associated with back-splicing (47,48). We searched circular RNA (circRNA) databases for the presence of circRNAs associated with *BRD2* exon 3b and *BRD3* exon 5b. Indeed, a circRNA corresponding to poison exon in *BRD2* was found in circBank (49) (circBank ID: hsa_circBRD2_001). The examination of the GTEx dataset with CIRCexplorer2 (50) also revealed exon 3b circularization in nine of the GTEx samples. No circRNAs were found for *BRD3* exon 5b, likely due to its low expression level.

Expression and splicing of poison exons

Panels of large-scale transcriptomic experiments offer a powerful tool for exploring gene expression and splicing profiles across clinically relevant conditions. Accordingly, we first characterized the patterns of BET genes' expression and splicing in healthy human tissues (GTEx). The $\log_{10}$-transformed median abundance of *BRD2* transcripts ($\log_{10}$TPM) in a tissue was negatively correlated with the median level of exon 3b inclusion (Ψ) in that tissue ($r_p = -0.34$, Figure 5A), and the negative trend was evident despite variation across samples (Supplementary Figure S8). A remarkably high abundance of *BRD2* transcripts and remarkably low Ψ values were observed in testis, where human *BRD2* was reported to be consistently expressed (51).

A similar relationship was observed when comparing the *BRD2* expression and splicing levels across a transcriptomic panel of human cancers (TCGA). The difference in $\log_{10}$-transformed median transcript abundance ($\Delta\log_{10}$TPM, tumor versus normal tissue) was negatively correlated ($r_p =$

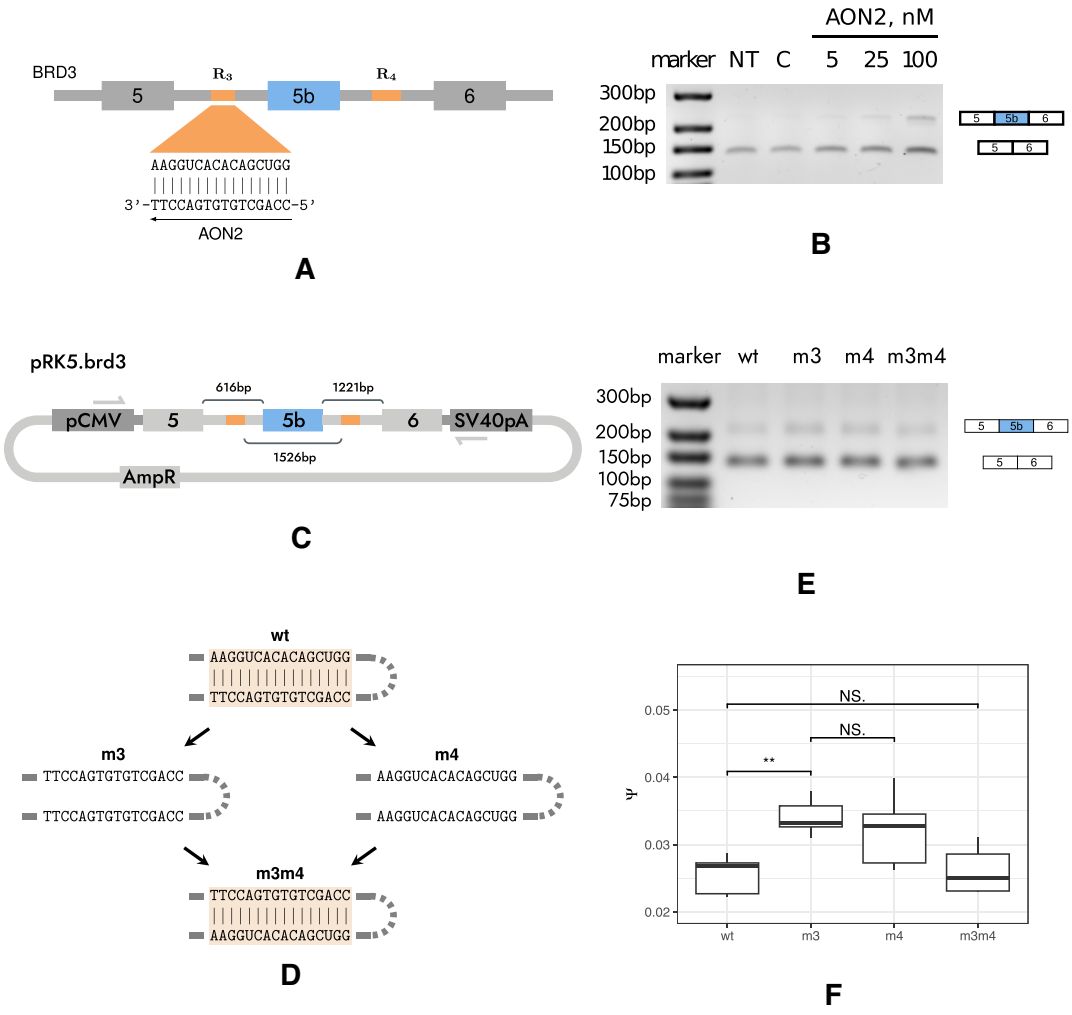

Figure 4. Validation of the RNA structure in *BRD3* gene. (**A**) AON2 is complementary to region R3. (**B**) Exon 5b inclusion rate increases when R3/R4 base pairings are blocked by AON2. (**C**) The minigene pRK5.BRD3 carrying a fragment of *BRD3* between exons 5 and 6. (**D**) Mutagenesis strategy is to create single disruptive mutants (m3 and m4) and a double compensatory mutant (m3m4). (**E**, **F**) Exon 5b inclusion rate increases in disruptive mutants but reverts to the WT in the compensatory double mutant. The notation in the legend is as in Figure 3.

−0.3) with the respective difference in the median exon 3b inclusion rate ($\Delta\Psi$) across 18 cancer types analyzed (Figure 5B and Supplementary Figure S9). Remarkably, the highest increase in exon 3b inclusion accompanied by a substantial drop in *BRD2* expression was observed in clear cell carcinoma of the kidney and renal papillary cell carcinoma, two cancer types in which the downregulation of *BRD2* was shown to be associated with poor survival rate (52).

While these observations are in agreement with the poison role of exon 3b, which should expectedly lead to a decrease in transcript abundance with its inclusion, a question remains whether RNA structure R1/R2 is involved in the regulation of exon 3b splicing. We addressed this question by examining two available datasets on the transcriptome response to the transcription elongation slowdown, one under α-amanitin treatment (26) and the other in the slow RNA Pol II mutant R749H (27). In both cases, the inclusion of exon 3b significantly declined (*P*-value = 0.002 and *P*-value = 0.02, respectively) when RNA Pol II speed was slowed down (Figure 5C and D). In accordance with poison exon skipping, the expression level of *BRD2* expectedly increases; however, the difference was not statistically significant (*P*-value = 0.15).

Poison exons in *BRD3* and *BRD4* are expressed at much lower levels as compared to *BRD2* exon 3b (Supplementary Figure S10), and their assessment is possible only in a fraction of tissues. In *BRD3*, the median transcript abundance and the median exon 5b inclusion rate are negatively associated (r_p = −0.25), while in *BRD4* the relationship is positive (r_p = 0.22), but driven mostly by an influential score representing testis tissue (Supplementary Figure S11). The response of poison exons in *BRD3* and *BRD4* to RNA Pol II slowdown cannot be reliably estimated due to low short-read coverage.

Discussion

In recent years, experimental and computational studies have demonstrated that RNA structure is critically important for alternative splicing regulation (26,30,53). While the overall function of alternative splicing can arguably be attributed to expanding the proteome diversity (54–56), the functional implication of altering the primary sequence of a particular protein in most cases remains undocumented, thereby limiting the interpretation of RNA structure's impact. Here, for the first time, we identified two PCCRs that control unproduc-

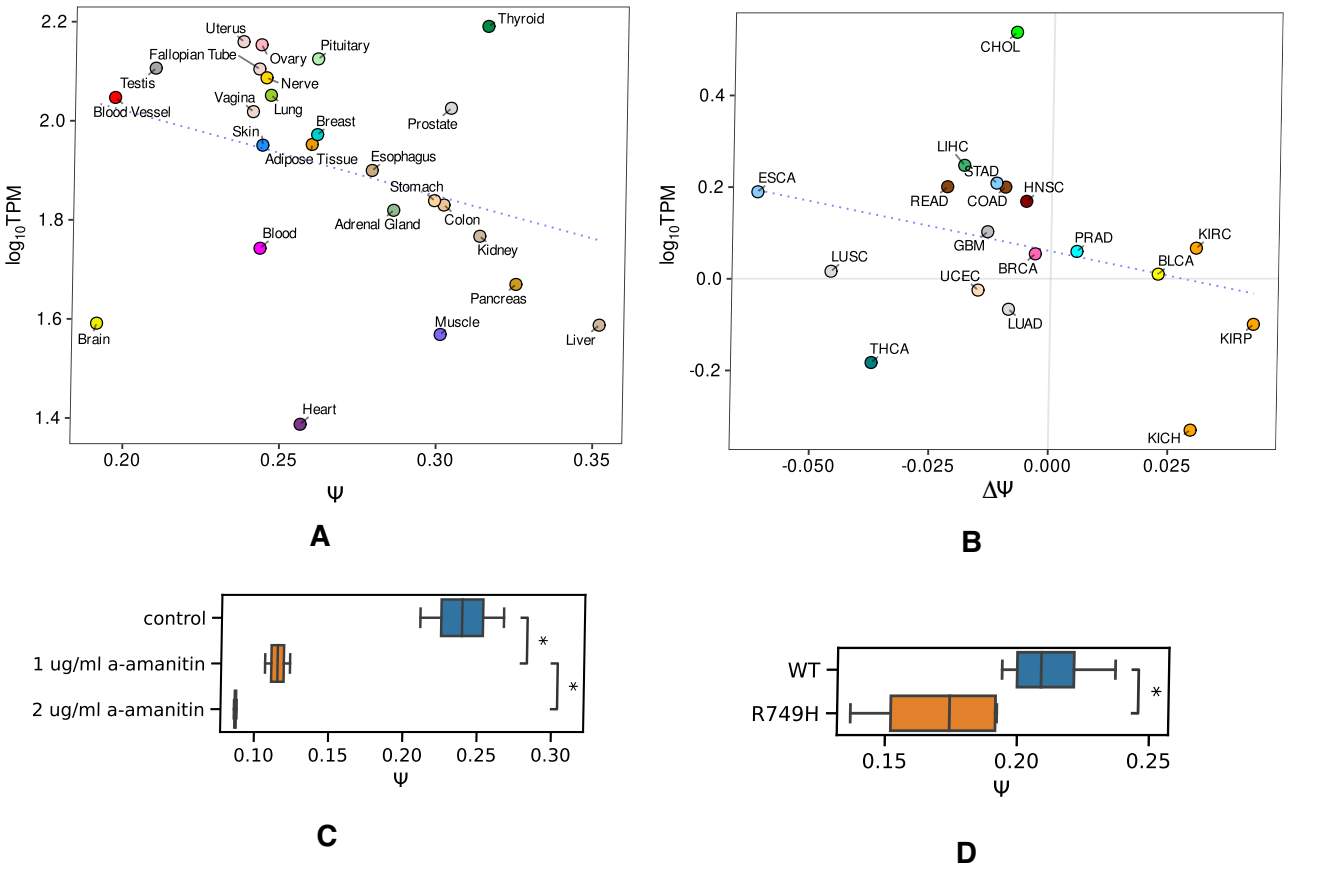

Figure 5. The patterns of *BRD2* expression and splicing. (**A**) The tissue-median rate of exon 3b inclusion (Ψ) is negatively associated ($r_p = -0.34$) with the $\log_{10}$-transformed tissue-median *BRD2* transcript abundance ($\log_{10}$TPM). The dotted line is the optimal least squares line. Tissue color codes are as in (68). (**B**) The difference in the median exon 3b inclusion rate (ΔΨ, tumor versus normal tissue) is negatively correlated ($r_p = -0.3$) with the difference in $\log_{10}$-transformed median transcript abundance ($\Delta\log_{10}$TPM). TCGA project color codes and abbreviations are as in (68). (**C**) The response of exon 3b inclusion (Ψ) to α-amanitin treatment. (**D**) Exon 3b inclusion rate (Ψ) in the WT and in the slow RNA Pol II mutant (R749H).

tive splicing representing an important example, in which the function of RNA structure can be directly attributed to post-transcriptional regulation of gene expression rather than to changes in the protein product itself.

Paralogous genes that arise through duplication and divergence often maintain a considerable degree of similarity not only between their encoded proteins but also between *cis*-regulatory elements and regulatory control mechanisms (57). In particular, this is true for serine–arginine (SR)-rich splicing factors, many of which evolved through duplications and contain homologous *cis*-regulatory elements that are associated with unproductive splicing (19). On the other hand, partial duplication of complementary sequences represents a general evolutionary mechanism for the generation of competing RNA structures that regulate mutually exclusive splicing (58). Therefore, genomic duplications naturally occur at the crossroads of unproductive splicing and RNA structure evolution.

Surprisingly, in the case of *BRD2* and *BRD3*, the regulatory poison exons are located in introns spanning between nonhomologous exons. This suggests that either *BRD2* and *BRD3* acquired them independently or each independently lost one of them in the evolution from the common ancestor. The fact that *BRD4* contains a poison exon but does not have RNA structure around it, and furthermore that *BRDT* and *fs(1)h*, an invertebrate homolog of BET proteins, do not have any annotated NMD isoforms, strongly indicated that the former scenario took place. Furthermore, the conserved complementary sequences surrounding poison exons in *BRD2* and *BRD3* share no sequence similarity with each other. All these observations suggest that the trait represented by regulatory RNA structures around poison exons is a result of convergent evolution. Rapid loss and reacquisition of poison exons (23) and independent origins of competing RNA secondary structures that control mutually exclusive splicing of tandemly duplicated exons (59) suggest that convergent evolution of RNA structures regulating unproductive splicing may extend far beyond the examples presented here.

In searching for the driving force of this convergent evolution, one may conjecture that RNA structures could regulate unproductive splicing through a mechanism related to transcription elongation rate. Slower RNA Pol II elongation rate allows sufficient time for RNA structure to fold, which, in turn, could lead to skipping of the looped-out exon. Such a mechanism was reported for the *ATE1* gene, which contains a pair of ultra-long-range complementary regions that control splicing of mutually exclusive exons (44). NELFE, a factor linked to RNA Pol II pausing (60–62), could be responsible for poison exon skipping and increased expression of *BRD2* and *BRD3* in testis. SR-rich splicing factors often implement a negative feedback loop that downregulates the productive splice isoform in response to elevated expression of the gene product (46). A similar feedback loop may also exist in *BRD2*,

however, acting through alternative splicing rather than RNA Pol II slowdown since *BRD2* does not appear to alter the transcription elongation rate itself (63).

The example of *BRD2* demonstrates that regulatory RNA structure may extend beyond PCCRs reported here, as the intron downstream of exon 3b contains a polymorphic microsatellite, the number of GT repeats in which negatively correlates with the rate of exon 3b inclusion (21). In general, self-base-pairing sequences such as GT tracts strongly affect splicing rate due to RNA secondary structure formation (64). While RNA structures formed by R1/R2 and R3/R4 were identified on the basis of evolutionary conservation, base pairings that are important for unproductive splicing may well exist in mRNAs of other BET family members, however, outside of conserved regions. This, and the extent to which RNA structure fits into the complex regulatory landscape of unproductive splicing and long ultraconserved elements associated with it, remains a question for future studies.

Studying mechanisms underlying BET-specific functions has far-reaching therapeutic implications as abnormal expression of these proteins leads to oncological, metabolic and cardiovascular disorders (65–67). The approach based on synthetic AONs was proven effective in targeting unproductive splicing, particularly in bromodomain proteins. For instance, AONs that promote skipping of poison exon 14a, which lead to increased *BRD9* mRNA degradation in tumors, help to restore *BRD9* protein levels and reverse tumor growth (22). In contrast, AONs targeting RNA structure elements in *BRD2* and *BRD3* offer a unique opportunity to not only suppress but also increase poison exon inclusion therapeutically. More importantly, the evidence for convergent evolution of poison exons and RNA structures in *BRD2* and *BRD3* provides an orthogonal view on the unproductive splicing regulation (68) in these and many other paralogous genes.

Conclusion

This study for the first time describes RNA structures that regulate unproductive splicing. Poison exons in *BRD2* and *BRD3*, of which the latter is a cryptic exon and was not annotated before, represent an example of convergent evolution that led to independent acquisition of poison exons and regulatory RNA structures. This study provides important implications for selective modulation of *BRD2* and *BRD3* expression in therapeutic applications.

Data availability

The data underlying this article are available in the article and in its online supplementary material.

Supplementary data

Supplementary Data are available at NARGAB Online.

Acknowledgments

The results presented here are in part based on the data generated by the TCGA Research Network (https://www.cancer.gov/tcga) and data obtained from the GTEx Portal and dbGaP accession number phs000424/GRU on 10 December 2018. The authors acknowledge Prof. Sergei Spirin for insightful discussions on BET family phylogeny.

Author contributions: D.D.P. designed and supervised the study; D.D.P. and S.M. performed data analysis; M.P., M.V. and D.S. performed the experiments; D.D.P., S.M. and M.P. wrote the first draft of the manuscript. All authors edited the final version of the manuscript.

Funding

Russian Science Foundation [21-64-00006].

Conflict of interest statement

None declared.

References

1. Jones,M.H., Numata,M. and Shimane,M. (1997) Identification and characterization of BRDT: a testis-specific gene related to the bromodomain genes RING3 and *Drosophilafsh*. *Genomics*, **45**, 529–534.
2. Lygerou,Z., Conesa,C., Lesage,P., Swanson,R.N., Ruet,A., Carlson,M., Sentenac,A. and Séraphin,B. (1994) The yeast BDF1 gene encodes a transcription factor involved in the expression of a broad class of genes including snRNAs. *Nucleic Acids Res.*, **22**, 5332–5340.
3. Dey,A., Ellenberg,J., Farina,A., Coleman,A.E., Maruyama,T., Sciortino,S., Lippincott-Schwartz,J. and Ozato,K. (2000) A bromodomain protein, MCAP, associates with mitotic chromosomes and affects G_2-to-M transition. *Mol. Cell. Biol.*, **20**, 6537–6549.
4. Wang,N., Wu,R., Tang,D. and Kang,R. (2021) The BET family in immunity and disease. *Signal Transduct. Target. Ther.*, **6**, 23.
5. Werner,M.T., Wang,H., Hamagami,N., Hsu,S.C., Yano,J.A., Stonestrom,A.J., Behera,V., Zong,Y., Mackay,J.P. and Blobel,G.A. (2020) Comparative structure–function analysis of bromodomain and extraterminal motif (BET) proteins in a gene-complementation system. *J. Biol. Chem.*, **295**, 1898–1914.
6. Sanchez,R. and Zhou,M.M. (2009) The role of human bromodomains in chromatin biology and gene transcription. *Curr. Opin. Drug Discov. Dev.*, **12**, 659–665.
7. Huang,M., Zeng,S., Zou,Y., Shi,M., Qiu,Q., Xiao,Y., Chen,G., Yang,X., Liang,L. and Xu,H. (2017) The suppression of bromodomain and extra-terminal domain inhibits vascular inflammation by blocking NF-κB and MAPK activation. *Br. J. Pharmacol.*, **174**, 101–115.
8. Paillisson,A., Levasseur,A., Gouret,P., Callebaut,I., Bontoux,M., Pontarotti,P. and Monget,P. (2007) Bromodomain testis-specific protein is expressed in mouse oocyte and evolves faster than its ubiquitously expressed paralogs BRD2, -3, and -4. *Genomics*, **89**, 215–223.
9. Denis,G.V., McComb,M.E., Faller,D.V., Sinha,A., Romesser,P.B. and Costello,C.E. (2006) Identification of transcription complexes that contain the double bromodomain protein Brd2 and chromatin remodeling machines. *J. Proteome Res.*, **5**, 502–511.
10. Stonestrom,A.J., Hsu,S.C., Jahn,K.S., Huang,P., Keller,C.A., Giardine,B.M., Kadauke,S., Campbell,A.E., Evans,P., Hardison,R. C., *et al.* (2015) Functions of BET proteins in erythroid gene expression. *Blood*, **125**, 2825–2834.
11. Xu,L., Chen,Y., Mayakonda,A., Koh,L., Chong,Y.K., Buckley,D.L., Sandanaraj,E., Lim,S.W., Lin,R.Y., Ke,X.Y., *et al.* (2018) Targetable BET proteins- and E2F1-dependent transcriptional program maintains the malignancy of glioblastoma. *Proc. Natl Acad. Sci. U.S.A.*, **115**, E5086–E5095.
12. Ghari,F., Quirke,A.M., Munro,S., Kawalkowska,J., Picaud,S., McGouran,J., Subramanian,V., Muth,A., Williams,R., Kessler,B., *et al.* (2016) Citrullination–acetylation interplay guides E2F-1 activity during the inflammatory response. *Sci. Adv.*, **2**, e1501257.

13. LeRoy,G., Rickards,B. and Flint,S.J. (2008) The double bromodomain proteins Brd2 and Brd3 couple histone acetylation to transcription. *Mol. Cell*, **30**, 51–60.
14. Cheung,K.L., Kim,C. and Zhou,M.M. (2021) The functions of BET proteins in gene transcription of biology and diseases. *Front. Mol. Biosci.*, **8**, 728777.
15. Shang,E., Wang,X., Wen,D., Greenberg,D.A. and Wolgemuth,D.J. (2009) Double bromodomain-containing gene Brd2 is essential for embryonic development in mouse. *Dev. Dyn.*, **238**, 908–917.
16. Houzelstein,D., Bullock,S.L., Lynch,D.E., Grigorieva,E.F., Wilson,V.A. and Beddington,R.S. (2002) Growth and early postimplantation defects in mice deficient for the bromodomain-containing protein Brd4. *Mol. Cell. Biol.*, **22**, 3794–3802.
17. Shao,Z., Zhang,R., Khodadadi-Jamayran,A., Chen,B., Crowley,M.R., Festok,M.A., Crossman,D.K., Townes,T.M. and Hu,K. (2016) The acetyllysine reader BRD3R promotes human nuclear reprogramming and regulates mitosis. *Nat. Commun.*, **7**, 10869.
18. Shen,H., Li,J., Xie,X., Yang,H., Zhang,M., Wang,B., Kent,K.C., Plutzky,J. and Guo,L.W. (2021) BRD2 regulation of sigma-2 receptor upon cholesterol deprivation. *Life Sci. Alliance*, **4**, e201900540.
19. Lareau,L.F., Inada,M., Green,R.E., Wengrod,J.C. and Brenner,S.E. (2007) Unproductive splicing of SR genes associated with highly conserved and ultraconserved DNA elements. *Nature*, **446**, 926–929.
20. Ni,J.Z., Grate,L., Donohue,J.P., Preston,C., Nobida,N., O'Brien,G., Shiue,L., Clark,T.A., Blume,J.E. and Ares,M. (2007) Ultraconserved elements are associated with homeostatic control of splicing regulators by alternative splicing and nonsense-mediated decay. *Genes Dev.*, **21**, 708–718.
21. Shang,E., Cui,Q., Wang,X., Beseler,C., Greenberg,D.A. and Wolgemuth,D.J. (2011) The bromodomain-containing gene BRD2 is regulated at transcription, splicing, and translation levels. *J. Cell. Biochem.*, **112**, 2784–2793.
22. Inoue,D., Chew,G.L., Liu,B., Michel,B.C., Pangallo,J., D'Avino,A.R., Hitchman,T., North,K., Lee,S.C., Bitner,L., *et al.* (2019) Spliceosomal disruption of the non-canonical BAF complex in cancer. *Nature*, **574**, 432–436.
23. Lareau,L.F. and Brenner,S.E. (2015) Regulation of splicing factors by alternative splicing and NMD is conserved between kingdoms yet evolutionarily flexible. *Mol. Biol. Evol.*, **32**, 1072–1079.
24. Dobin,A., Davis,C.A., Schlesinger,F., Drenkow,J., Zaleski,C., Jha,S., Batut,P., Chaisson,M. and Gingeras,T.R. (2013) STAR: ultrafast universal RNA-seq aligner. *Bioinformatics*, **29**, 15–21.
25. Harrow,J., Frankish,A., Gonzalez,J.M., Tapanari,E., Diekhans,M., Kokocinski,F., Aken,B.L., Barrell,D., Zadissa,A., Searle,S., *et al.* (2012) GENCODE: the reference human genome annotation for The ENCODE Project. *Genome Res.*, **22**, 1760–1774.
26. Kalmykova,S., Kalinina,M., Denisov,S., Mironov,A., Skvortsov,D., Guigó,R. and Pervouchine,D. (2021) Conserved long-range base pairings are associated with pre-mRNA processing of human genes. *Nat. Commun.*, **12**, 2300.
27. Fong,N., Kim,H., Zhou,Y., Ji,X., Qiu,J., Saldi,T., Diener,K., Jones,K., Fu,X.D. and Bentley,D.L. (2014) Pre-mRNA splicing is facilitated by an optimal RNA polymerase II elongation rate. *Genes Dev.*, **28**, 2663–2676.
28. Liao,Y., Smyth,G.K. and Shi,W. (2014) featureCounts: an efficient general purpose program for assigning sequence reads to genomic features. *Bioinformatics*, **30**, 923–930.
29. Pervouchine,D.D., Knowles,D.G. and Guigó,R. (2013) Intron-centric estimation of alternative splicing from RNA-seq data. *Bioinformatics*, **29**, 273–274.
30. Margasyuk,S., Kalinina,M., Petrova,M., Skvortsov,D., Cao,C. and Pervouchine,D.D. (2023) RNA *in situ* conformation sequencing reveals novel long-range RNA structures with impact on splicing. *RNA*, **29**, 1423–1436.
31. Pertea,M., Pertea,G.M., Antonescu,C.M., Chang,T.C., Mendell,J.T. and Salzberg,S.L. (2015) StringTie enables improved reconstruction of a transcriptome from RNA-seq reads. *Nat. Biotechnol.*, **33**, 290–295.
32. Siepel,A., Bejerano,G., Pedersen,J.S., Hinrichs,A.S., Hou,M., Rosenbloom,K., Clawson,H., Spieth,J., Hillier,L.W., Richards,S., *et al.* (2005) Evolutionarily conserved elements in vertebrate, insect, worm, and yeast genomes. *Genome Res.*, **15**, 1034–1050.
33. Huerta-Cepas,J., Szklarczyk,D., Heller,D., Hernández-Plaza,A., Forslund,S.K., Cook,H., Mende,D.R., Letunic,I., Rattei,T., Jensen,L.J., *et al.* (2019) eggNOG 5.0: a hierarchical, functionally and phylogenetically annotated orthology resource based on 5090 organisms and 2502 viruses. *Nucleic Acids Res.*, **47**, D309–D314.
34. Letunic,I. and Bork,P. (2021) Interactive Tree Of Life (iTOL) v5: an online tool for phylogenetic tree display and annotation. *Nucleic Acids Res.*, **49**, W293–W296.
35. Martin,F.J., Amode,M.R., Aneja,A., Austine-Orimoloye,O., Azov,A.G., Barnes,I., Becker,A., Bennett,R., Berry,A., Bhai,J., *et al.* (2023) Ensembl 2023. *Nucleic Acids Res.*, **51**, D933–D941.
36. Edgar,R.C. (2004) MUSCLE: multiple sequence alignment with high accuracy and high throughput. *Nucleic Acids Res.*, **32**, 1792–1797.
37. Waterhouse,A.M., Procter,J.B., Martin,D.M., Clamp,M. and Barton,G.J. (2009) Jalview Version 2—a multiple sequence alignment editor and analysis workbench. *Bioinformatics*, **25**, 1189–1191.
38. Chomczynski,P. and Sacchi,N. (1987) Single-step method of RNA isolation by acid guanidinium thiocyanate–phenol–chloroform extraction. *Anal. Biochem.*, **162**, 156–159.
39. de Ronde,M.W.J., Ruijter,J.M., Lanfear,D., Bayes-Genis,A., Kok,M.G.M., Creemers,E.E., Pinto,Y.M. and Pinto-Sietsma,S.J. (2017) Practical data handling pipeline improves performance of qPCR-based circulating miRNA measurements. *RNA*, **23**, 811–821.
40. Touznik,A., Maruyama,R., Hosoki,K., Echigoya,Y. and Yokota,T. (2017) SMN2 gene and restore SMN protein expression in type 1 SMA fibroblasts. *Sci. Rep.*, **7**, 3672.
41. Belkina,A.C. and Denis,G.V. (2012) BET domain co-regulators in obesity, inflammation and cancer. *Nat. Rev. Cancer*, **12**, 465–477.
42. Pervouchine,D.D. (2018) Towards long-range RNA structure prediction in eukaryotic genes. *Genes (Basel)*, **9**, 302.
43. Blanchette,M., Kent,W.J., Riemer,C., Elnitski,L., Smit,A.F., Roskin,K.M., Baertsch,R., Rosenbloom,K., Clawson,H., Green,E.D., *et al.* (2004) Aligning multiple genomic sequences with the threaded blockset aligner. *Genome Res.*, **14**, 708–715.
44. Kalinina,M., Skvortsov,D., Kalmykova,S., Ivanov,T., Dontsova,O. and Pervouchine,D.D. (2021) Multiple competing RNA structures dynamically control alternative splicing in the human ATE1 gene. *Nucleic Acids Res.*, **49**, 479–490.
45. Lykke-Andersen,S., Chen,Y., Ardal,B.R., Lilje,B., Waage,J., Sandelin,A. and Jensen,T.H. (2014) Human nonsense-mediated RNA decay initiates widely by endonucleolysis and targets snoRNA host genes. *Genes Dev.*, **28**, 2498–2517.
46. Pervouchine,D., Popov,Y., Berry,A., Borsari,B., Frankish,A. and Guigó,R. (2019) Integrative transcriptomic analysis suggests new autoregulatory splicing events coupled with nonsense-mediated mRNA decay. *Nucleic Acids Res.*, **47**, 5293–5306.
47. Wang,Y. and Wang,Z. (2015) Efficient backsplicing produces translatable circular mRNAs. *RNA*, **21**, 172–179.
48. Pervouchine,D.D. (2019) Circular exonic RNAs: when RNA structure meets topology. *Biochim. Biophys. Acta Gene Regul. Mech.*, **1862**, 194384.
49. Liu,M., Wang,Q., Shen,J., Yang,B.B. and Ding,X. (2019) Circbank: a comprehensive database for circRNA with standard nomenclature. *RNA Biol.*, **16**, 899–905.
50. Zhang,X.O., Dong,R., Zhang,Y., Zhang,J.L., Luo,Z., Zhang,J., Chen,L.L. and Yang,L. (2016) Diverse alternative back-splicing and alternative splicing landscape of circular RNAs. *Genome Res.*, **26**, 1277–1287.

51. Thorpe,K.L., Gorman,P., Thomas,C., Sheer,D., Trowsdale,J. and Beck,S. (1997) Chromosomal localization, gene structure and transcription pattern of the ORFX gene, a homologue of the MHC-linked RING3 gene. *Gene*, **200**, 177–183.
52. Lu,J., Qian,C., Ji,Y., Bao,Q. and Lu,B. (2021) Gene signature associated with bromodomain genes predicts the prognosis of kidney renal clear cell carcinoma. *Front. Genet.*, **12**, 643935.
53. Cai,Z., Cao,C., Ji,L., Ye,R., Wang,D., Xia,C., Wang,S., Du,Z., Hu,N., Yu,X., *et al.* (2020) RIC-seq for global *in situ* profiling of RNA–RNA spatial interactions. *Nature*, **582**, 432–437.
54. Tress,M.L., Abascal,F. and Valencia,A. (2017) Alternative splicing may not be the key to proteome complexity. *Trends Biochem. Sci.*, **42**, 98–110.
55. Blencowe,B.J. (2017) The relationship between alternative splicing and proteomic complexity. *Trends Biochem. Sci.*, **42**, 407–408.
56. Guigó,R. (2023) Genome annotation: from human genetics to biodiversity genomics. *Cell Genom.*, **3**, 100375.
57. Maconochie,M., Nonchev,S., Morrison,A. and Krumlauf,R. (1996) Paralogous Hox genes: function and regulation. *Annu. Rev. Genet.*, **30**, 529–556.
58. Ivanov,T. M. and Pervouchine,D.D. (2018) An evolutionary mechanism for the generation of competing RNA structures associated with mutually exclusive exons. *Genes (Basel)*, **9**, 356.
59. Yue,Y., Hou,S., Wang,X., Zhan,L., Cao,G., Li,G., Shi,Y., Zhang,P., Hong,W., Lin,H., *et al.* (2017) Role and convergent evolution of competing RNA secondary structures in mutually exclusive splicing. *RNA Biol.*, **14**, 1399–1410.
60. Vos,S.M., llmann,D., Caizzi,L., Hofmann,K.B., Rombaut,P., Zimniak,T., Herzog,F. and Cramer,P. (2016) Architecture and RNA binding of the human negative elongation factor. *eLife*, **5**, e14981.
61. Yamaguchi,Y., Inukai,N., Narita,T., Wada,T. and Handa,H. (2002) Evidence that negative elongation factor represses transcription elongation through binding to a DRB sensitivity-inducing factor/RNA polymerase II complex and RNA. *Mol. Cell. Biol.*, **22**, 2918–2927.
62. Fujinaga,K., Irwin,D., Huang,Y., Taube,R., Kurosu,T. and Peterlin,B.M. (2004) Dynamics of human immunodeficiency virus transcription: P-TEFb phosphorylates RD and dissociates negative effectors from the transactivation response element. *Mol. Cell. Biol.*, **24**, 787–795.
63. Hnilicová,J., Hozeifi,S., Stejskalová,E., Dušková,E., Poser,I., Humpolíčková,J., Hof,M. and Staněk,D. (2013) The C-terminal domain of Brd2 is important for chromatin interaction and regulation of transcription and alternative splicing. *Mol. Biol. Cell*, **24**, 3557–3568.
64. Hefferon,T.W., Groman,J.D., Yurk,C.E. and Cutting,G.R. (2004) A variable dinucleotide repeat in the CFTR gene contributes to phenotype diversity by forming RNA secondary structures that alter splicing. *Proc. Natl Acad. Sci. U.S.A.*, **101**, 3504–3509.
65. Sarnik,J., Popławski,T. and Tokarz,P. (2021) BET proteins as attractive targets for cancer therapeutics. *Int. J. Mol. Sci.*, **22**, 11102.
66. Wu,D. and Duan,Q. (2022) Roles of bromodomain extra terminal proteins in metabolic signaling and diseases. *Pharmaceuticals (Basel)*, **15**, 1032.
67. Borck,P.C., Guo,L.W. and Plutzky,J. (2020) BET epigenetic reader proteins in cardiovascular transcriptional programs. *Circ. Res.*, **126**, 1190–1208.
68. Mironov,A., Petrova,M., Margasyuk,S., Vlasenok,M., Mironov,A.A., Skvortsov,D. and Pervouchine,D.D. (2023) Tissue-specific regulation of gene expression via unproductive splicing. *Nucleic Acids Res.*, **51**, 3055–3066.

Received: September 21, 2023. **Revised:** December 13, 2023. **Editorial Decision:** December 19, 2023. **Accepted:** December 28, 2023
© The Author(s) 2024. Published by Oxford University Press on behalf of NAR Genomics and Bioinformatics.
This is an Open Access article distributed under the terms of the Creative Commons Attribution-NonCommercial License (http://creativecommons.org/licenses/by-nc/4.0/), which permits non-commercial re-use, distribution, and reproduction in any medium, provided the original work is properly cited. For commercial re-use, please contact journals.permissions@oup.com